

DOI: 10.1134/S0869864321040028

Numerical simulation of underexpanded supersonic jets impingement on an inclined flat plate*

A.S. Epikhin^{1,2} and T.G. Elizarova³

¹*Ivannikov Institute for System Programming RAS, Moscow, Russia*

²*Bauman Moscow State Technical University, Moscow, Russia*

³*Keldysh Institute of Applied Mathematics RAS, Moscow, Russia*

E-mail: andrey.epikhin@bk.ru

*(Received February 18, 2021; revised February 18, 2021;
accepted for publication May 18, 2021)*

The paper presents the results of numerical simulation of complex shock-wave structures arising from an under-expanded jets impingement on an inclined flat plate. The plate deflection angles equal to 45°, 60°, and 90° are investigated, which corresponds to different types of shock waves interference. The gas-dynamic characteristics are calculated using the OpenFOAM software package with the QGDFoam solver. This solver based on a system of regularized (quasi-gas dynamic) equations. The numerical simulation results of the flowfields and pressure distributions at the plate are compared against the results of the Kurganov–Tadmor scheme and with experimental data. The features of the applied numerical approach for simulation of complex shock-wave structures with triplet points, contact discontinuities, and low-entropy flows are identified.

Keywords: numerical simulation, underexpanded jet interaction, shock-wave structures, regularized (quasi-gas dynamic) equations, QGDFoam, OpenFOAM.

Introduction

The interest in the investigation of gas outflow into a vacuum is motivated by a wide range of scientific and industrial applications. For example, engineering of space vehicles often faces the situation when the onboard elements (antennas, plates, protective shields) are allocated on a plane, cylindrical, or spherical surfaces and subjected by the injected jets. There are a large number of papers devoted to the study of free supersonic underexpanded jets [1–5]. Typically, the studies of jet-plate interaction were arranged, as a rule, for the case of a single axisymmetric jet [6–11]. Therefore, there is a shortage of research for the interaction of two underexpanded jets with obstacles. The interaction of the jet flow with protruding elements is accompanied by complex shock-wave structures with 3D flow separation zones. The study of that kind of flow requires expensive experimental equipment. According to [12, 13], there are six types of shock waves interactions. The authors of this study made the analysis of real

* The study was financially supported by the Russian Science Foundation, Project No. 19-11-00169. The research was performed using the equipment of the Collective Use Center “Complex for simulation and data processing for mega-class research facilities” at NRC “Kurchatov Institute”.

experimental data focused on the flow patterns for every flow type; approximates for gas-dynamic parameters were given. These papers dealt with uniform flows.

In last years, these kinds of problems are solved using the CFD software packages [14–16]. However, for the effective use of such software, it is necessary to validate it. The numerical simulation of gas dynamics for high-altitude jets is a difficult task. Primarily, this is due to a complicated geometry of simulation domains dictated by a design of joint devices on the vehicle. Other factors are multi-blocked jets, different nozzle sizes, and factors that change the gas dynamic features: interference between shock-wave, contact discontinuities, low-entropy flows, zones of separation, local instabilities, etc. The choice of numerical algorithm for solving conservation equations is an independent problem. This is essential for solution characteristics and matching to the initial problem statement.

Many of the available explicit numerical methods based on Godunov-type schemes (HLL, HLLC, Roe, etc.) can produce instabilities for simulation of the shocks. It is known that the Kurganov–Tadmor scheme avoids this problem, but it has a significant dissipation [17]. One of the shortages of these algorithms is the limited area of applicability at the values of Mach number less than 1 that reduces the accuracy for the regions with the subsonic flow. An alternative to these approaches is using hybrid schemes [18] and algorithms based on quasi-gas dynamic (QGD) equations [19]. These regularized equations for gas dynamics are the analogs of Navier–Stokes equations and can be applied to a wide range of flow problems. The QGD algorithms (based on these equations) are distinguished by the uniformity of differential approximations, simple implementations, and physically reasonable and controllable numerical dissipation. This approach is instrumental for solving the flow of ideally expanded jets [20]. The QGD algorithm was used for the simulation of unsteady interaction with an obstacle placed normally to the jet axis [21]. It also works for problems with the interaction of parallel jets.

This paper presents the flowfields of two underexpanded jets impinging on an inclined flat plate at various plate angles. The three types of shock waves interference occurring for the plate oriented to the axial plane by 45°, 60°, and 90° have been investigated. The simulations were performed with the open-source software OpenFOAM, which is widely used for the simulation of supersonic jets in recent years. The pressure distributions over the plate are compared with the results from [14] calculated with rhoCentralFoam solver which is based on Kurganov–Tadmor scheme and the experimental data presented in that paper.

1. Governing equations

The simulation was based on a numerical algorithm for solving QGD equations which are implemented in the QGDfoam solver of the OpenFOAM package [22, 23]. The QGD system included the conservation equations for mass (1), momentum (2), and energy (3) [19, 22]:

$$\frac{\partial \rho}{\partial t} + \nabla \cdot \mathbf{j}_m = 0, \quad (1)$$

$$\frac{\partial \rho \mathbf{u}}{\partial t} + \nabla \cdot (\mathbf{j}_m \otimes \mathbf{u}) + \nabla p = \nabla \cdot \mathbf{\Pi}, \quad (2)$$

$$\frac{\partial E}{\partial t} + \nabla \cdot \left(\frac{\mathbf{j}_m}{\rho} (E + p) \right) + \nabla \cdot \mathbf{q} = \nabla \cdot (\mathbf{\Pi} \cdot \mathbf{u}), \quad (3)$$

$$\mathbf{j}_m = \rho(\mathbf{u} - \mathbf{w}),$$

$$\mathbf{\Pi} = \mathbf{\Pi}_{NS} + \mathbf{\Pi}_{QGD},$$

$$\mathbf{q} = \mathbf{q}_{NS} + \mathbf{q}_{QGD},$$

where ρ is the density, \mathbf{u} is the velocity vector, \mathbf{j}_m is the mass flux, p is the pressure, E is the total energy, $\mathbf{\Pi}$ is the viscous stress tensor, \mathbf{q} is the heat flux, $\mathbf{\Pi}_{NS}$, \mathbf{q}_{NS} are the viscous

stress tensor and heat flux for the Navier–Stokes equation; \mathbf{w} , $\mathbf{\Pi}_{\text{QGD}}$, \mathbf{q}_{QGD} are the additional dissipative terms in corresponding equations that proportional to coefficient τ [22]:

$$\begin{aligned}\mathbf{w} &= \tau/\rho \cdot (\nabla \cdot (\rho \mathbf{u} \otimes \mathbf{u}) + \nabla p), \\ \mathbf{\Pi}_{\text{QGD}} &= \tau \cdot (\mathbf{u} \otimes (\rho \mathbf{u} \cdot \nabla \mathbf{u} + \nabla p) + \hat{\mathbf{I}} \cdot (\mathbf{u} \cdot \nabla p + \gamma \cdot p \cdot (\nabla \cdot \mathbf{u}))), \\ \mathbf{q}_{\text{QGD}} &= \tau \cdot \mathbf{u} \cdot \rho \cdot (\mathbf{u} \cdot \nabla (p/\rho(\gamma-1)) + p \mathbf{u} \cdot \nabla (1/\rho)),\end{aligned}$$

where $\hat{\mathbf{I}}$ is a unit tensor, and γ is the heat capacity ratio. The QGD equation system is an extension of the classic Navier–Stokes equations: it comprises the extra terms proportional to a small coefficient τ with the dimension of time. When the τ parameter tends to zero, the QGD system becomes the Navier–Stokes equation system. The parameter τ in dimensionless form is proportional to the Knudsen number. For the compressible gases, the value τ is too small for practical use and cannot provide the required stability of the numerical algorithm. In this case, the role of the mean free path in this numerical algorithm is taken by the grid spatial step:

$$\tau = \alpha_{\text{QGD}} \frac{\Delta}{c},$$

where α_{QGD} is a constant varying from 0 to 1 and being the adjustment parameter for the QGD algorithm, Δ is the computational grid step, and c is the speed of sound. When we solve the problems with high Mach and Reynolds numbers, the τ -derived dissipation can be not sufficient. Therefore, the artificial viscosity is introduced into the system as a coefficient in the viscous stress tensor:

$$\mu \rightarrow \mu + \text{Sc}_{\text{QGD}} \cdot p \cdot \tau,$$

where Sc_{QGD} is the scheme parameter that ensures stability at a high local Mach number. For the case of calculating the high-gradient flows (the shocks), one can use the dynamic definition for Sc_{QGD} parameter (as it was outlined in [24]):

$$\text{Sc}_{\text{QGD}} = \frac{\sum (\delta_p/\delta_n) \delta x}{\sum (2p)}, \quad (4)$$

where $p = (p_n - p_p)/2$, $(\delta_p/\delta_n) \delta x = (p_p + p_n)$, p_p and p_n are the pressures at the centers of the previous (p) and next (n) cells.

2. Problem settings

The problem considers two jets that outflow from conical nozzles with exit diameter D_a : the jet axes are parallel and distanced by $a/D_a=1.8$. The flow impinges onto a plate allocated at the distance of $H/D_a = 5.9$ from the nozzle exit and oriented at angles $\theta = 45^\circ, 60^\circ$, or 90° to the axis (Fig. 1). The jets are imitated by air flow ($\gamma = 1.4$). The Mach number at the nozzle exit is $M = 3$, and the cone angle is 10° , the jet pressure ratio is $n = p_a/p_\infty = 30$, where p_a is the pressure at the nozzle exit, p_∞ is the ambient pressure. At the initial time, the ambient flow is stationary.

The computational setup with the $x0z$ symmetry plane is considered. The parameter Sc_{QGD} was evaluated by formula (4), and $\text{Sc}_{\text{QGD}(\text{wall})} = 0$ on the plate. The fixed values for pressure, temperature, and velocity are assigned for the nozzle exit. The plate surface is an adiabatic wall with no-slip velocity conditions on the surface. On the free boundaries, soft zero gradient conditions are used. The problem is solved in unsteady formulation.

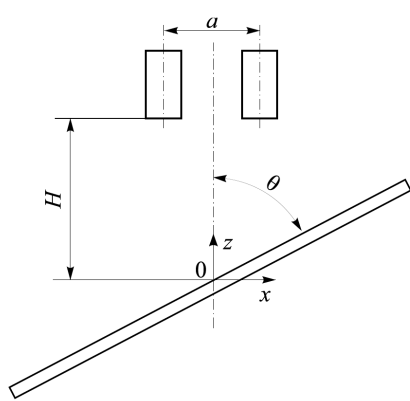


Fig. 1. Definitions of geometric parameters.

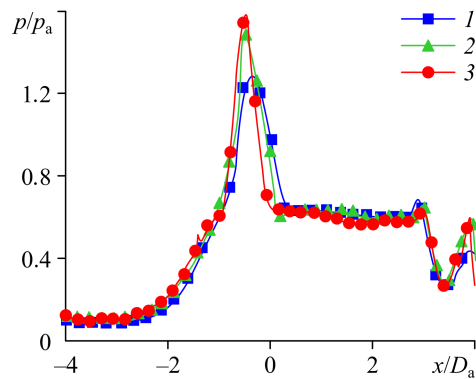


Fig. 2. Pressure distributions along the plate centerline for different grid resolution. 1 — 20 CPD, 2 — 40 CPD, 3 — 80 CPD.

Numerical simulations were performed on a 3D hexahedron mesh. The grid was refined in the area of interaction between two jets. The total number of cells were $1.8 \cdot 10^6$, $8 \cdot 10^6$, and $32 \cdot 10^6$ approximately which corresponds to the resolution in the refinement area equal to 20, 40, and 80 cells per nozzle exit diameter (CPD). Therefore, the minimal cells size in the jets interaction zone for these three variants were $\Delta = D_a/20$, $D_a/40$, $D_a/80$, respectively. The convergence of numerical solutions for calculated pressure distributions for a plate with $\theta = 60^\circ$ is plotted in Fig. 2.

It was found that the grid condensing allows to obtain a better resolution for pressure peaks. The comparison of three similar calculations reveals a better convergence for higher cells numbers. The difference between the pressure top values for the cases of meshes with CPD equal to 40 and 80 is about 6 %.

3. Results and discussion

It should be noted that the simulated flow in the region of interaction of the jet flow with the plate is pulsated and the structure of interfering shocks moves periodically. This varies the position and magnitude of pressure maximum on the plate surface. The unsteady features of flow in this area are caused by physical processes and are not covered by this research. In this paper, the time-average results for QGDFoam and rhoCentralFoam solvers are presented for 80 CPD.

Figure 3 presents the structure of interaction between two underexpanded jets impinging onto a plate inclined at the angle of $\theta = 90^\circ$. At the initial outflow zone, the two underexpanded

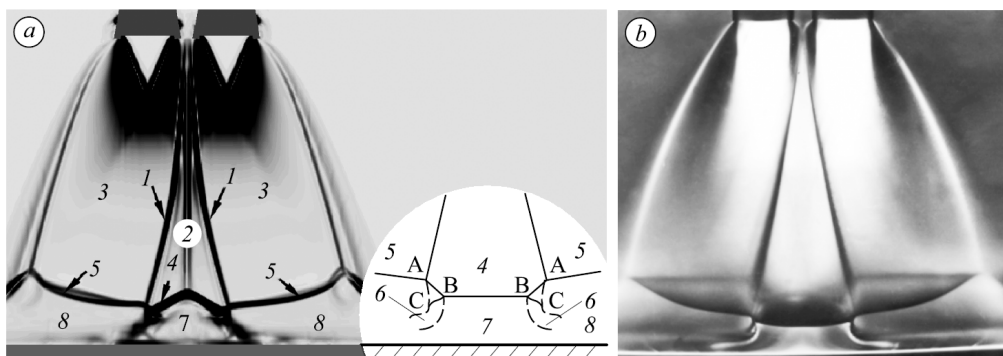
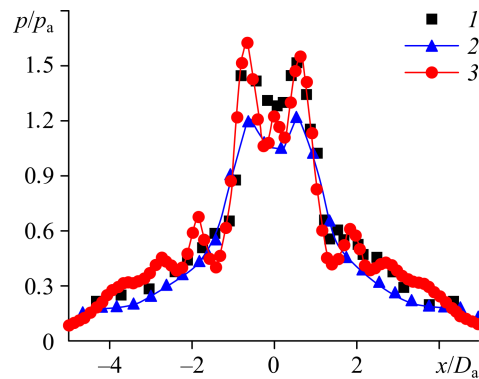


Fig. 3. Flowfields of the interaction of two jets with a horizontal plate. a — density gradient map, b — Schlieren image [14].

Fig. 4. Pressure distributions along the plate oriented at $\theta = 90^\circ$. Experiment (1); calculations using rhoCentralFoam (2) and QGDFoam (3) solvers.



jets converge ahead of the interaction plane which produces jet shock 1 with embracement of the compressed gas layer 2. The interaction of the undisturbed part of jet 3 and compressed gas layer 2 with the plate occurs strong plate shocks 4 and 5, respectively. The interference between these elements and shock 1 produces a configuration with triplet points A and B. The contact discontinuities originating from points A and B are the boundaries of low-entropy flows 6, the shape and position of this object are defined by a ratio of pressure in zones 7 and 8. If the pressure in zone 7 is higher than in zone 8, the flow turns to the low-pressure zone and cannot reach the plate surface. If these pressures are close, the low-entropy flows are diffused on the plate surface and spread along the interaction zone avoiding zone 8. The shape and position of low-entropy flows and the pressure ratio determine the gas flow rate from zone 7 and the flow pattern, which in turn, determines the pressure on the plate. The interaction-neighboring zone 7 behind the shock wave (between two low-entropy flows) is the zone with elevated pressure over the plate (Fig. 4). The pressure sharp declines beyond this zone. The jet periphery exhibits the interference of the barrel shock with the plate shock wave 5 which produces the triple shock configuration. The simulation curve is plotted slightly lower than the experimental data for the zone of jet interaction. The reason can be in the fact that experimental results were obtained for impingement of a slightly heated jet; this would eliminate the condensed phase in the nozzle, but this is not guaranteed for the jets flow. The presence of a condensed phase in the jet changes the expansion ratio and the positions of shocks [14]. It should be noted that the pressure distribution simulated using the rhoCentralFoam solver is much lower than the results based on the QGD algorithm. The point is the Kurganov–Tadmor scheme is a more dissipative one than the QGD algorithm. This “smears out” the region of contact discontinuities (the boundaries of low-entropy flows 6) and leads to a freer (compared to experiment) gas outflow from zone 7, therefore, the pressure becomes lower than experimental data.

The variation in inclination angle θ disturbs the flow pattern symmetry relative to the plane of jets interaction. This changes the shock-wave structure in different jet impingement areas. Figure 5 shows the structure of interaction of two underexpanded jets with a plate oriented at

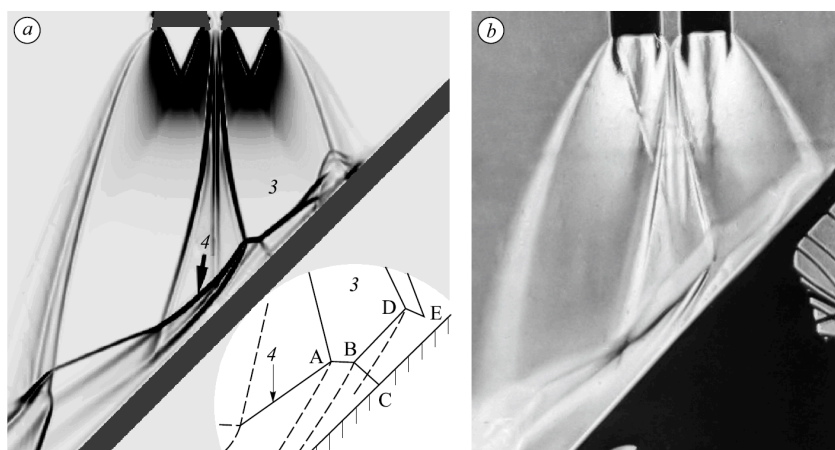


Fig. 5. Flowfields of the interaction of jets with the plate oriented at 45° . a — density gradient map, b — Schlieren image [14].

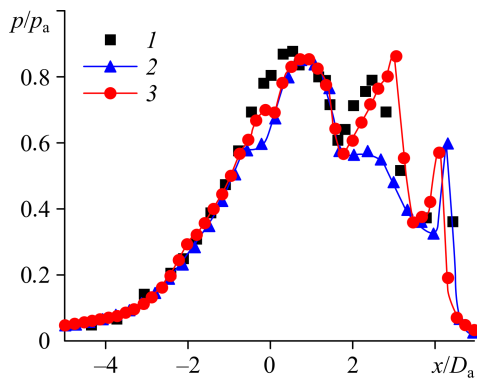


Fig. 6. Pressure distributions on the plate with $\theta = 45^\circ$. Experimental data (1) and calculations using the rhoCentralFoam (2) and QGDFoam (3) solvers.

the angle of $\theta = 45^\circ$. The interference of shocks produces a configuration with two triple points A and B, meanwhile, point B is actually a point of “bending” for plate shock AD, occurring due to interaction of undisturbed part of jet 3 with the plate surface. Point B is the origin for the intrinsic shock, and point D is for contact discontinuity. The length of shock AB is rather moderate for this range of underexpansion ratio. In the high-pressure zone past the shock wave 4 the experimental and simulated pressure distributions are close by magnitude (Fig. 6). The contact discontinuity originating from point D (Fig. 5) is pushed to the plane surface by the flow that passed the shock BD. The experimental pressure profile exhibits the second high-pressure area. The calculations demonstrate that the gas flow that passed through the upper tail shock DE is decelerated on the plate with forming of a slip line: here the pressure has peak-shaped behavior. This high-level pressure was not obtained in experiments due to rare drainage. The simulation pressure values in the first area comply with two simulation approaches. Meanwhile, the second area is better described with the QGD algorithm. In turn, the incomppliance of pressure value with the Kurganov–Tadmor scheme calculations can be explained by the absence of the triple point B and the intermediate shock BC in the simulated structure [14]. As it was mentioned, the BC impingement place coincides with the high-pressure zone.

Figure 7 shows the structure on the interaction of two underexpanded jets with a plate oriented at the angle of $\theta = 60^\circ$. According to the Schlieren image for the plate oriented at $\theta = 60^\circ$ (Fig.7b), the contact discontinuity from point A and the supersonic flow after the shock AB impinge on the plate surface and produce an intermediate shock BC, this ensures the flow rotation in parallel to the plate. At that, the crossing of this shock with the shock wave AF is followed by the shock bending and originates the triplet point B. A similar shock wave structure was observed in simulations as well (Fig. 7a). For this type of impingement, both experimental and simulation data of the pressure distributions on the plate are shown in Fig. 8. One feature of pressure distribution is the observation of a steady pressure in the subsonic area past the shock AD. The pressure profile simulated using the Kurganov–Tadmor scheme is slightly

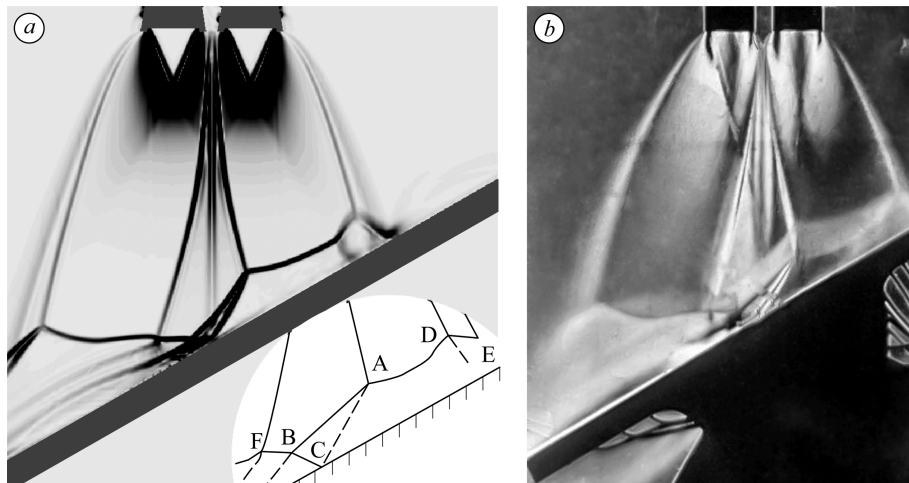
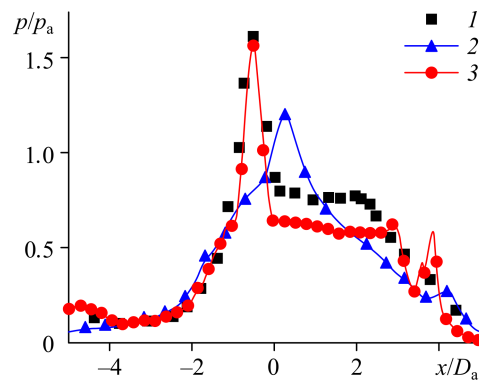


Fig. 7. Flowfields of the interaction of jets with the plate oriented at 60° . a — density gradient map, b — Schlieren image [14].

Fig. 8. Pressure distributions on the plate with $\theta = 60^\circ$.

Experimental data (1) and calculations using the rhoCentralFoam (2) and QGDFoam (3) solvers

different from the results of the QGD algorithm and experimental data. As was mentioned above, it is due to a dissipative feature of the Kurganov–Tadmor scheme: the A-originating contact discontinuity is smoothed and moves further. This would alter the position of interaction between BC and AF shocks. This discrepancy in the flowfield significantly changes (qualitatively and quantitatively) the behavior of pressure on the plate [14]. The QGD approach gives more accurate flowfields and pressure distributions, the results comply better with the experimental data. Note that the convergence of this solution as a function of grid resolution is plotted in Fig. 2.



Conclusion

The validation for solving the QGD equations has been performed using the numerical simulation of shock-wave structures with triplet points, contact discontinuity, and low-entropy flows. The study showed that the QGD algorithm reproduces the flow structures accurately, it can depict without extra smoothing some individual shocks and triplet configurations. The qualitative and quantitative compliance for simulated and experimental pressure data are observed.

Comparison of available data with the results of the application of the Kurganov–Tadmor scheme (a variant of Godunov’s method) shows that the last one solver is more dissipative and exhibits a stronger smoothing of discontinuities. However, this approach has less computational cost in the existing version of the OpenFOAM package. Therefore, the Kurganov–Tadmor scheme can be recommended for practical problems taking into account complex shock-wave structures in the absence of contact discontinuities or for cases where contact discontinuities have an insignificant effect on the result. For the other situations, the QGD approach or high-order schemes are preferable. The QGD approach makes it possible to determine the interaction of long contact discontinuities due to the nonlinear nature of artificial dissipation. This helps in the simulation of flowfields and pressure distributions in high resolution both for the supersonic and subsonic flows.

References

1. E.S. Love, C.E. Grigsby, L.P. Lee, and M.J. Woodling, Experimental and theoretical studies of axisymmetric free jets, NASA Technical Report. 1959.
2. E. Franquet, V. Perrier, S. Gibout, and P. Bruel, Free underexpanded jets in a quiescent medium: a review, Progress in Aerospace Sci., 2015, Vol. 77, P.25–53.
3. Yu.I. Gerasimov and V.N. Yarygin, Jet expansion of ideal and real gases from axisymmetric nozzles. Similarity matters. 1. Outflow of jets into vacuum, Physical-Chemical Kinetics in Gas Dynamics, 2012, Vol. 13, No. 1, P. 1–22.
4. V.I. Zapryagaev, N.P. Kiselev, and A.A. Pivovarov, Gasdynamic structure of an axisymmetric supersonic underexpanded jet, Fluid Dynamics, 2015, Vol. 50, No. 1, P. 95–107.
5. V.I. Zapryagaev, N.P. Kiselev, and D.A. Gubanov, Shock-wave structure of supersonic jet flows, Aerospace, 2018, Vol. 5, No. 2, P. 60–1–60–18.
6. P.J. Lamont and B.L. Hunt, The impingement of underexpanded, axisymmetric jets on perpendicular and inclined flat plates, J. Fluid Mech., 1980, Vol. 100, No. 3, P. 471–511.
7. D.T. Nguyen, B. Maher, and Y. Hassan, Effects of nozzle pressure ratio and nozzle-to-plate distance to flowfield characteristics of an under-expanded jet impinging on a flat surface, Aerospace, 2019, Vol. 6, No. 1, .P. 4-1–4-28.

8. **Y. Nakai, N. Fujimatsu, and K. Fujii**, Experimental study of underexpanded supersonic jet impingement on an inclined flat plate, *AIAA J.*, 2006, Vol. 44, No. 11, P. 2691–2699.
9. **I.P. Ginzburg, B.G. Semiletenko, V.S. Terpigor'ev, and V.N. Uskov**, Some singularities of supersonic underexpanded jet interaction with a plane obstacle, *J. Engng Phys.*, 1970, Vol. 19, P. 1081–1084.
10. **K.N. Volkov, V.N. Emelyanov, A.V. Efremov, and A.I. Tsvetkov**, Flow structure and pressure oscillations during the interaction of a supersonic underexpanded gas jet with a tubular cavity, *Techn. Phys.*, 2020, Vol. 90, No. 8, P. 1204–1216.
11. **Yu.I. Gerasimov, V.N. Yarygin, A.N. Krylov, and B.A. Sagdullin**, Modeling of the flow structure in a composite jet behind two thrusters located near the spacecraft case, *Thermophysics and Aeromechanics*, 2009, Vol. 16, No. 3, P. 375–383.
12. **B. Edney**, Anomalous heat transfer and pressure distributions on blunt bodies at hypersonic speeds in the presence of an impinging shock, Aeronautical Research Institute of Sweden, FFA Report No. 115, 1968. .
13. **B.A. Zemlyanskii, V.V. Lunev, V.I. Vlasov, A.B. Gorshkov, and G.N. Zalogin**, Convective Heat Transfer of Flight Vehicles, Fizmatlit, Moscow, 2014.
14. **V.V. Voronin, A.S. Epikhin, and N.E. Khramov**, Numerical simulation of gas dynamics in complex shock-wave structures accompanying high-altitude jet interactions of operating spacecraft, *Kosmonavtika & Raketostroyeniye*, 2018, Vol. 100, No. 1, P. 118–126.
15. **K. McIlroy and K. Fujii**, Computational analysis of supersonic underexpanded jets impinging on an inclined flat plate, 37th AIAA Fluid Dynamics Conference and Exhibit, AIAA Paper, 2007, No. 2007–3859.
16. **A.O. Beketaeva, Ye.S. Moiseyeva, and A.Zh. Naimanova**, Numerical simulations of shock-wave interaction with a boundary layer in the plane supersonic flows with jet injection, *Thermophysics and Aeromechanics*, 2016, Vol. 23, No. 2, P. 173–184.
17. **A. Kurganov and E. Tadmor**, New high-resolution semi-discrete central schemes for Hamilton–Jacobi equations, *J. Comp. Phys.*, 2000, Vol. 160, No. 2, P. 720–742.
18. **M.V. Kraposhin, M. Banholzer, M. Pfitzner, and I.K. Marchevsky**, A hybrid pressure-based solver for nonideal single-phase fluid flows at all speeds, *Inter. J. Numer. Methods in Fluids*, 2018, Vol. 88, No. 2, P. 79–99.
19. **T.G. Elizarova**, Quasi-gas Dynamic Equations. Berlin: Springer, 2009.
20. **A. Epikhin and M. Kraposhin**, Prediction of the free jet noise using quasi-gas dynamic equations and acoustic analogy, *Lecture Notes in Comput. Sci.*, 2020, Vol. 12143, P. 217–227.
21. **I.A. Graur, T.G. Elizarova, and J.C. Lengrand**, Investigation of shock configurations induced by a plume impinging upon a perpendicular plate, in *Proceedings of the 23rd Inter. Symp. on Shock Waves*, 2001, P. 677–683.
22. **M.V. Kraposhin, E. Smirnova, T.G. Elizarova, and M.A. Istomina**, Development of a new OpenFOAM solver using regularized gas dynamic equations, *Computers and Fluids*, 2018, Vol. 166, P. 163–175.
23. **QGDFoam solver**: <https://github.com/unicfdlab/QGDsolver>.
24. **F. Ducros, V. Ferrand, F. Nicoud, C. Weber, D. Darracq, C. Gacherieu, and T. Poinso**, Large-eddy simulation of the shock, Turbulence interaction, *J. Comput. Phys.*, 1999, Vol. 152, No. 2, P. 517–549.